

Identification of Backlash in Mechanical Systems

T. Tjahjowidodo, F. Al-Bender, H. Van Brussel
K.U.Leuven, Department Mechanical Engineering
Celestijnenlaan 300 B, B-3001, Heverlee, Belgium
email: tegoeh.tjahjowidodo@mech.kuleuven.ac.be

Abstract

Estimation of the modal parameters of mechanical systems or structures is usually achieved by applying the well-known Frequency Response Function (FRF) method to experimental data obtained from free vibration after a shock excitation of the system or forced vibration using a variety of excitation signals. This method is however limited only to linear systems. The problem becomes more complex when nonlinear systems have to be identified. If the nonlinear system is 'well-behaved', i.e. if it shows periodic response to a periodic excitation, 'skeleton' identification techniques may be used to estimate the modal parameters, in function of the amplitude and frequency of excitation. However, under certain excitation conditions, chaotic behaviour might occur so that the response is aperiodic. In that case, chaos quantification techniques, such as Lyapunov exponent, are proposed in the literature. This paper deals with the application of the aforementioned nonlinear identification techniques to an experimental mechanical system with backlash. It compares and contrasts Hilbert transforms with Wavelet analysis in case of skeleton identification showing their possibilities and limitations. Chaotic response, which appears under certain excitation conditions and could be used as backlash signature, is dealt with both by a simulation study and by experimental signal analysis after application of appropriate filtration techniques.

1 Introduction

Estimation of modal parameters of linear mechanical structures is usually carried out by utilizing the Frequency Response Function (FRF) method using an experimental analysis such as free vibration with shock excitation or forced vibration with step or chirp excitation. However, there is a limitation that only linear dynamic systems can be tested through these methods. To overcome this difficulty, many researchers [1,2] introduced nonlinear vibration system identification based on the Hilbert transform.

By definition [3], the Hilbert transform is a mathematical transform that shifts each frequency component of the instantaneous spectrum by $\pi/2$ without affecting the magnitude. Feldman [5,6] has proposed methods of FreeVib and ForceVib to identify instantaneous modal parameters (natural frequencies, damping characteristics and their dependencies on a vibration amplitude and frequency). FreeVib is suitable for identifying the modal parameters of the system by free vibration analysis. However, when the system is well damped, ForceVib is more suitable.

These identification techniques proves to be very simple and effective, yet it has some limitations. Ruzzene et al. [8] show that the envelope and instantaneous frequency estimation in Hilbert transform technique introduce more errors when high damping is present in the system. An improvement can be achieved when Wavelet Transform is used instead of the Hilbert Transform to approximate the envelope signal and its instantaneous frequency. Wavelet Transform is a time-frequency representation (TFR) technique, which is developed as an alternative approach to the Short Time Fourier Transform to overcome the resolution problem. Staszewski [12] extensively describes this technique in his theoretical study. However, there are hardly any instances in the literature of the application of these techniques to real systems. This paper presents such a practical application to a mechanical system with a backlash component.

The aforementioned identification technique, based on skeleton reconstruction, actually is based on the classical assumption that the output of a nonlinear structure is periodic if the input is periodic. Under some special conditions however, this assumption is no longer valid, namely in the case of chaotic behaviour,

and special techniques need to be developed in order to quantify such behaviour. No definition of chaos is universally accepted, but the general meaning tends to convey little of the strict definition [13]: *Chaos is aperiodic long-term behavior in a deterministic system that exhibits sensitive dependence on initial conditions*. Sensitive dependence on initial condition means that two trajectories starting very close together will rapidly diverge from each other, and thereafter have totally different futures. The divergence (or convergence) of two neighbouring trajectories can be used to quantify the degree of chaos, namely the Lyapunov exponent (λ). In our case, the Lyapunov Exponent is proposed to be a mechanical signature of the backlash component. Lin et al. [22] show theoretically that under certain excitations, a simple nonlinear mechanical system with backlash might manifest chaotic vibration. Our paper confirms experimentally the possible presence of chaotic response in a real mechanical system and characterises it.

In short, this paper thus applies various nonlinear system identification techniques to an experimental mechanical system with backlash and compares and evaluates them. Section 2 presents and discusses identification techniques using Hilbert and Wavelet transforms, for regular response, and chaotic system quantification for chaotic response. In this section theoretical perspectives will also be presented including special noise reduction technique for chaotic signal. Section 3 describes the experimental system with a backlash element, applies the aforementioned techniques to analyse it and discusses the results obtained. Finally, some conclusions are drawn in section 4.

2 Theoretical Basis

2.1 Skeleton Identification

The skeleton technique enables us to identify the ‘instantaneous’ modal parameters, including restoring force and damping force, for a certain class of nonlinear systems, through analysing their free or forced response by methods such as the ones described in the following.

2.1.1 Hilbert Transform [5,6]

A large number of signals, including vibration of nonlinear system can be converted to an analytic signal in complex-time and represented in the form of the combination of envelope and instantaneous phase [1,2]:

$$Y(t) = y(t) + j\tilde{y}(t) = A(t) \cdot e^{j\varphi(t)} \quad (2.1)$$

where $\tilde{y}(t)$ is the Hilbert Transform of the real-valued signal $y(t)$, $Y(t)$ is an analytic signal in complex-time function, $A(t)$ and $\varphi(t)$ are an envelope (amplitude) signal and an instantaneous phase respectively.

We now consider that the forced vibration equation of a single-degree-of-freedom system could be written as:

$$\ddot{y} + 2h_0(A)\dot{y} + \omega_0^2(A)y = F/m \quad (2.2)$$

where y is the response signal, F is the forced excitation signal, m is the mass of the system, h_0 and ω_0 are symmetrical viscous damping and stiffness characteristic of the system, respectively, which depend on the amplitude, A . According to the main properties of non-overlapping spectra of Hilbert Transform, Feldman [6] shows that equation (2.2) can be converted by Hilbert Transform to the complex form:

$$\ddot{Y} + 2h_0(A)\dot{Y} + \omega_0^2(A)Y = F/m \quad (2.3)$$

where $Y(t) = A(t) \cdot e^{j\varphi(t)}$ is an analytic signal of a solution of the system and $F(t)$ is the analytic signal of the forced excitation in complex-time form.

Substituting the analytic signal forms of $Y(t)$ and $F(t)$ together with the two derivatives of $Y(t)$ in equation (2.3), the representation of the corresponding modal parameters can be derived [6]:

$$\omega_0^2(t) = \omega^2 + \frac{\alpha(t)}{m} - \frac{\beta(t)\dot{A}}{A\omega m} - \frac{\ddot{A}}{A} + \frac{2\dot{A}^2}{A^2} + \frac{\dot{A}\dot{\omega}}{A\omega} \quad (2.4a)$$

$$h_0(t) = \frac{\beta(t)}{2\omega m} - \frac{\dot{A}}{A} - \frac{\dot{\omega}}{2\omega} \quad (2.4b)$$

where ω is time derivative of the instantaneous phase φ , while α and β are the real and imaginary parts of the ratio $\frac{F(t)}{Y(t)} = \alpha(t) + j\beta(t)$, respectively.

2.1.2 Wavelet Transform

Wavelet analysis is done in a similar way to the Short Time Fourier Transform (STFT), in the sense that the signal is multiplied by a function (i.e. *mother wavelet*, similar to the window function in STFT), and the transform is computed separately for different segments of the time-domain signal. The main difference between Wavelet Transform and STFT is the width of the 'window' in Wavelet Transform, which changes as the transform is computed for every single spectral component. Therefore, Wavelet analysis allows the use of long time intervals where we want more precise low-frequency information, and shorter regions where we want high-frequency information.

The Wavelet Transform of real-value signal $y(t)$ is defined as follows:

$$W(s, \tau) = \frac{1}{\sqrt{|s|}} \int_{-\infty}^{+\infty} y(t) \psi^* \left(\frac{t - \tau}{s} \right) dt \quad (2.5)$$

As seen in the equation above, the transformed signal is a function of **translation**, τ , which corresponds directly to time, **scale/dilation** (s), which relates to frequency information indirectly, and $\psi(t)$ as a **mother wavelet**.

Different researchers have proposed several families of mother wavelet functions. The mother wavelet function, which will be used in this paper, is the popular function of Complex Morlet Wavelet [9]:

$$\psi(t) = \sqrt{\pi f_b} \cdot e^{j\omega_c t} \cdot e^{-t^2/f_b} \quad (2.6)$$

where f_b is the bandwidth parameter and $\omega_c = 2\pi f_c$ is the centre frequency.

Envelope and Instantaneous Frequency Extraction from Wavelet Transform

Energy density distribution over the (s, τ) scale-translation plane can be represented by the square of the modulus of Wavelet transform. The energy of a signal is mainly concentrated on that plane around the so-called ridge of the wavelet transform. This ridge is directly related to the instantaneous frequency of the signal. Tchamitchian et al. [10] formulated the relation of the instantaneous frequency and the ridge as follows:

$$s = \frac{\dot{\phi}_c(0)}{\dot{\phi}(\tau)} \quad (2.7)$$

While assuming that the envelope $A(t)$ of equation (2.1) is slowly varying, Carmona et al. [11] approximate the modulus of Morlet-Wavelet transform for any given signal with slow varying envelope as:

$$|W(s, \tau)| \approx \frac{1}{\sqrt{|s|}} A(\tau) |\Psi^*(s\dot{\phi}(\tau))| \quad (2.8)$$

Thus, from equation (2.7), the instantaneous frequency of the analytical solution can be obtained from the ridge extraction of Wavelet transform. Once the ridge and instantaneous frequencies are known, the envelope of the signal $y(t)$ can be recovered following equation (2.8), and some modal parameters can be reconstructed following the same concept as in the Hilbert technique.

2.2 Detecting and Quantifying Chaos

Based on a unique property of chaotic behavior that two trajectories starting very close together will rapidly diverge from each other, the divergence (or convergence) of two neighboring trajectories can be used as chaos quantification measure, called the *Lyapunov Exponent* (λ).

For a system whose equations of motion are explicitly known, evaluating Lyapunov Exponent can be done in a straightforward way by observing the separation of two close initial trajectories on the attractor. But unfortunately this method cannot be applied directly to experimental data for the reason that we are not always dealing with two (or more) sets of experimental data that have closed initial condition. Reconstructing phase space from the time series with appropriate time delay and embedding dimension makes it possible to obtain an attractor whose Lyapunov spectrum is identical to that of the original attractor. Mathematically, the reconstructed phase space can be described as follows [14,15]:

$$y(k)=[S(k), S(k+\tau), S(k+2\tau), \dots, S(k+(d-1)\tau)] \quad (2.9)$$

where $S(k)$ is the time series from a single observation, τ represents appropriate time delay for phase space reconstruction, and d is a proper embedding dimension for phase space reconstruction

Now, if we choose two points in the reconstructed phase space whose temporal separation in the original time series is at least one 'orbital period', they may be considered as different trajectories on the attractor. Hence, the next step in determining the largest Lyapunov exponent for the time series is searching the nearest neighbor of certain points, in term of Euclidean distance, which are considered as fiducial trajectories.

In reconstructing the phase space of equation (2.9), we must make sure that the points in each dimension (coordinate) are independent each other. Therefore, time lag τ must be chosen so as to result in points that are not correlated to previously generated points. Time lag selection was done by utilizing *Average Mutual Information* (AMI) technique [19]. Analogically, the time delay may be considered as the time at which the auto-correlation function attains zero. However, the auto-correlation function measures rather the linear dependence between successive points.

The next following step is to recover the adequate number of coordinates d of the phase space. The idea of number of coordinates d is a dimension in which the geometrical structure of the phase space is completely unfolded. The most popular method for determining the embedding dimension in reconstructed phase-space is *False Nearest Neighbor* method [20]. Suppose the vector $y^{NN}(k)$ in dimension d is a false neighbor of $y(k)$, having arrived in its neighborhood by projection from a higher dimension, because the present dimension d does not unfold the attractor, then by going to the next dimension $d+1$, we may move this false neighbor out of the neighborhood of $y(k)$.

Similar to the idea of False Nearest Neighbor, Cao [17] proposed the mean value of $a(i,d)$:

$$E(d) = \frac{1}{N-d\tau} \sum_{i=1}^{N-d\tau} a(i,d) ; \text{ where } a(i,d) = R_{d+1}(k) / R_d(k) \quad (2.10)$$

where $R_d(k)$ is the Euclidean distance between the vector $y(k)$ to its neighbor in dimension d .

To investigate variation of $E(d)$ from d to $d+1$, Cao also defined: $E1(d) = E(d+1)/E(d)$ (2.11)

$E1(d)$ stops changing when d is greater than some particular value d_0 if the time series comes from an attractor, and its embedding dimension is d_0+1 .

2.2.1 Noise Reduction on Chaotic Signals

We shall see in section 3 that noise reduction is important for accurate estimation of the embedding dimension. Noise reduction techniques are closely related to the future prediction theory. For prediction we have no information about the quantity to be forecast other than the preceding measurement, while for noise reduction we have a noisy measurement to start with and we have the future values. Hence we aim to replace the noisy measurement with a set of 'prediction values' containing errors, which are on average less than the initial amplitude of the noise.

Suppose the time evolution of our observation is following a deterministic mapping function $F: x_{n+1} = F(x_n)$, which is not known to us. But however, our measurement data (s_n) are contaminated by noise:

$$s_n = x_n + \eta_n \tag{2.12}$$

where η_n is random noise with no correlation with signal x_n .

The noise reduction scheme is implemented as follows [20]: First, an embedding dimension m has to be chosen by using any method, such as False Nearest Neighbor. Using this information, we can construct an m -dimensional measurement signal $\{s_n\}$. Then for each embedding vector $\{s_n\}$, a neighborhood $\{U_\epsilon\}$ is formed and we may determine those which are close to s_n , let us say they are $\{s_n'\}$.

For each embedding vector $\{s_n\}$ a corrected middle coordinate $s_{n-m/2}$ is computed by averaging over the neighbourhood. The reason for using the middle coordinate in this data reduction method is related to the fact that the middle coordinate is assumed to be the most stable direction in a chaotic trajectory.

2.2.2 Theoretical Consideration and Simulation of Chaotic Response

A simple system, as shown in Figure 1, comprising a backlash spring is found to be chaotic under certain excitation conditions. Table 1 gives two sets of system’s parameters pertaining to chaotic behaviour, for certain excitation force specifications, where m is the mass of the system, k_1 and k_0 are stiffnesses, c is a damping coefficient, and x_0 the backlash (or play) size.

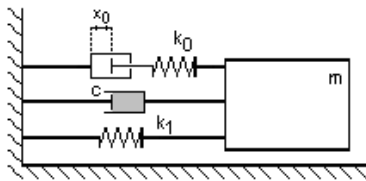


Figure 1. Nonlinear Mechanical System with Backlash component

	m (kg)	k_1 (N/m)	k_0 (N/m)	c (Ns/m)	x_0 (m)
CASE 1	1	0	40000	8	0.005
CASE 2	1	1000	31000	8	0.005

Table 1. Parameter sets of vibration system

It has been found that there exist certain sinusoidal excitation forces for CASE 1, with $A = |F| = 100$ N and for CASE 2 with $A = 240$ N, both at $\omega = 40$ rad/s, which cause the response to behave chaotically [22]. In order to examine the influence of each parameter on the nature of resulting response, dimensional is used to normalise the variables and reduce the number of parameters. By combining variables in dimensionless groups, one may gain more insight in the problem.

Thus, introducing new variables of time and displacement $\tau = \omega_0 t$ and $p = x / x_0$, where $\omega_0^2 = k_0 / m$, we may write the dynamics equation for CASE 1 ($k_1 = 0$) as follows:

$$m\omega_0^2 x_0 p'' + c\omega_0 x_0 p' + k_0 x_0 \bar{F}(p) = A \cos \omega t \tag{2.13}$$

where the primes indicate differentiation with respect to τ and F is the backlash spring function. This equation reduces to:

$$p'' + 2\zeta p' + \bar{F}(p) = \alpha \cos \omega t \tag{2.14}$$

where $2\zeta = \frac{c}{\sqrt{k_0 m}}$ and $\alpha = \frac{A}{k_0 x_0}$. That is to say that the problem is characterised by two parameters.

To see how chaotic motion evolves when the forcing amplitude decreases (or the backlash size increases), the relation between largest Lyapunov Exponential and the parameter of $1/\alpha$ has been generated for CASE 1 and is presented in Figure 2. Figure 3 shows bifurcation diagram of CASE 1, for $2\zeta = 0.04$, providing similar representation to Figure 2.

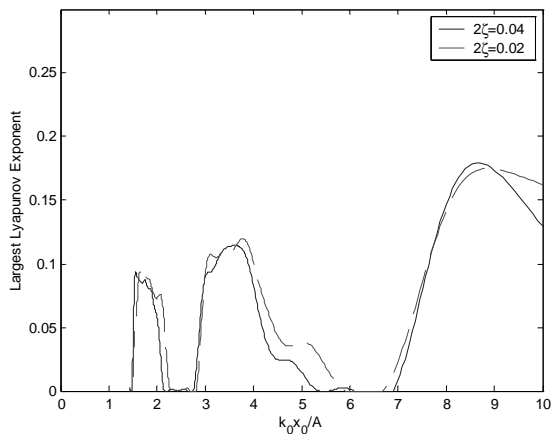


Figure 2. Largest Lyapunov Exponent vs $1/\alpha$

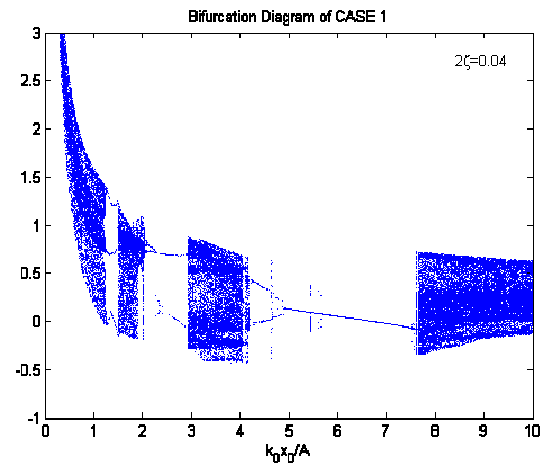


Figure 3. Bifurcation diagram of CASE 1

3 EXPERIMENTAL STUDY

3.1 Skeleton Identification

Experiment was conducted on the outer (second) link of a two-link mechanism as shown in Figure 4 and Figure 5. The aim of this experiment is to identify the backlash size of the second link joint. For this purpose, certain degree of backlash (approximately 1.5°) was introduced in the joint of this link. The first link was kept fix while the second one was made to oscillate over a certain range. This link was driven by a servomotor through a toothed belt and a harmonic drive.

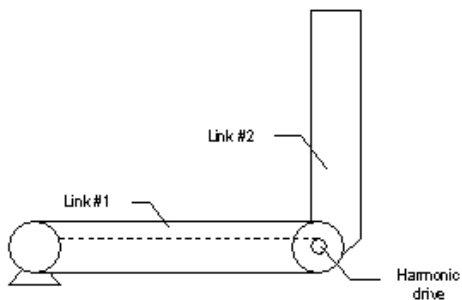


Figure 4. Schematic drawing of a two-link mechanism

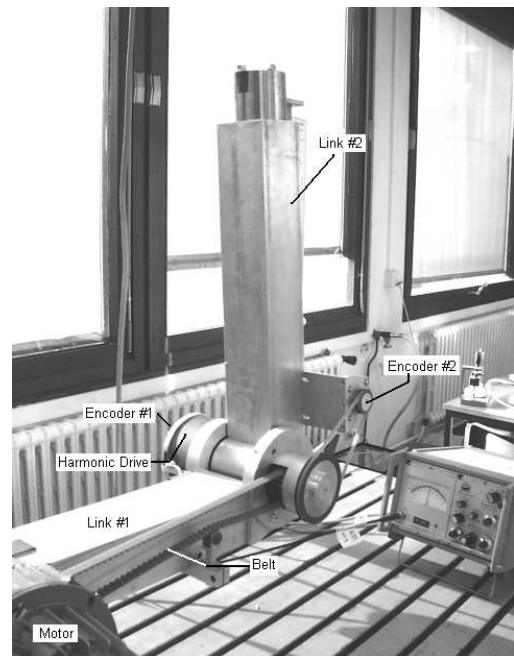


Figure 5. Setup of two-link mechanism

The vibration responses were measured with two rotary encoders. First encoder measured the angular motion input to the harmonic drive, and the second one measured the relative oscillation between first link and second link. Therefore, the first encoder might be considered to measure excitation input of a *base motion system* in displacement form, while the second encoder measured the response of the base motion system.

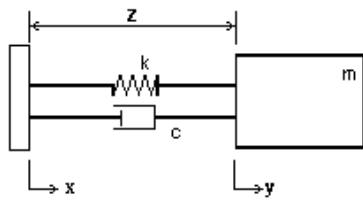


Figure 6. Base Motion System

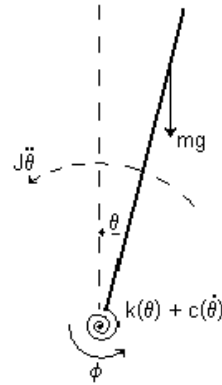


Figure 7. Force balance diagram of link #2

In the case of base motion system (Figure 6), where the excitation input is taken in the form of displacement, we need a little mathematical manipulation to solve the problem formulated in equation (2.2). The differential equation of displacement equation form for this problem can be written as:

$$\ddot{y} + 2h_0(A)\dot{y} + \omega_0^2(A)y = 2h_0(A)\dot{x} + \omega_0^2(A)x \tag{3.1}$$

where: x = displacement input.

If we introduce z as a relative motion between x and y ($z = y-x$), we may rewrite equation (3.1) as:

$$\ddot{z} + 2h_0(A)\dot{z} + \omega_0^2(A)z = -\ddot{x} \tag{3.2}$$

Taking $-\ddot{x}$ as input in equation (2.2), we can obviously identify the modal parameters of the system.

Schematic force balance of link #2 of the two-link system can be seen in Figure 7. The link is supported by a nonlinear backlash rotational spring and damper of its joint. The support of this link has a specified rotational motion of ϕ , which is referred to a displacement input and measured by the first encoder. Angular motion of link #2 is represented by θ .

The nonlinear differential equation of motion of the system shown in Figure 7 can be obtained easily. Referring to equation (3.1), and simplifying notations of $y = \theta$ and $x = \phi$, we get:

$$\ddot{y} + 2h_0(A)\dot{y} + \{\omega_0^2(A) - C\}y = 2h_0(A)\dot{x} + \omega_0^2(A)x \tag{3.3}$$

where $C = mgL/J$ is an additional stiffness due to the link weight, m is mass of the link, L is the coordinate of the centre of gravity of the link, and J equals the link's moment of inertia about its joint.

In the notation of equation (3.2), equation (3.3) can be rewritten as:

$$\ddot{z} + 2h_0(A)\dot{z} + \omega_0^2(A)z = -\ddot{x} + Cy, \quad (z = y-x) \tag{3.4}$$

If we refer to the transformation from displacement equation to complex-analytic signal form from reference [5], by analogy we can transform equation (3.4) into complex-analytic signal form:

$$\ddot{Z} + 2h_0(A)\dot{Z} + \omega_0^2(A)Z = -\ddot{X} + CY \tag{3.5}$$

3.1.1 Signal analysis

The experiments were taken by exerting linear chirp signal to the motor. Initial frequency of this signal is 0 Hz. The frequency continues to change at constant rate, and it reaches 12 Hz in 30 sec.

The oscillation response measured by encoder #1, which later will be considered as displacement input of second link, is depicted in Figure 8. Relative motion between second and first link can be seen in Figure 9.

Relative motion between responses measured by both encoders, where in equation (3.5) was represented by z , can be seen in Figure 10. It is clearly seen from that figure, that the relative motion is higher than the backlash size in the joint. In the figure, the dash lines represent size of the backlash. At time 16.25 sec, which corresponds approximately to 6.5 Hz of excitation frequency, the relative motion of the link falls far

below the size of backlash. This occurs due to insufficient energy of excitation. Such problem might cause unsatisfactory skeleton curve reconstruction, which is essential in modal parameter identification.

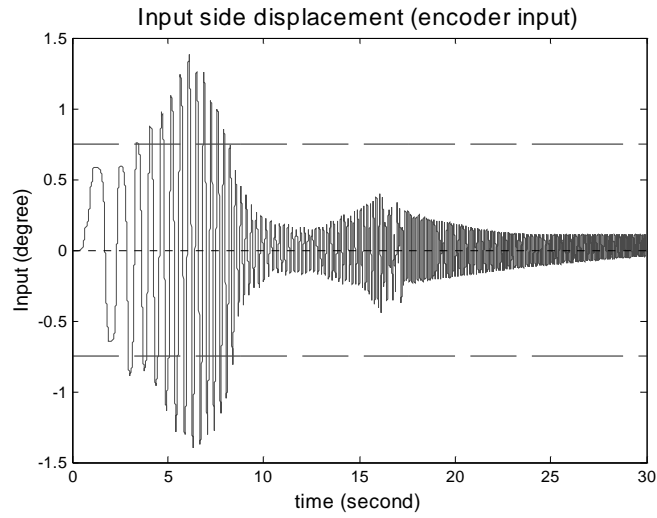


Figure 8. Oscillation measured by encoder #1

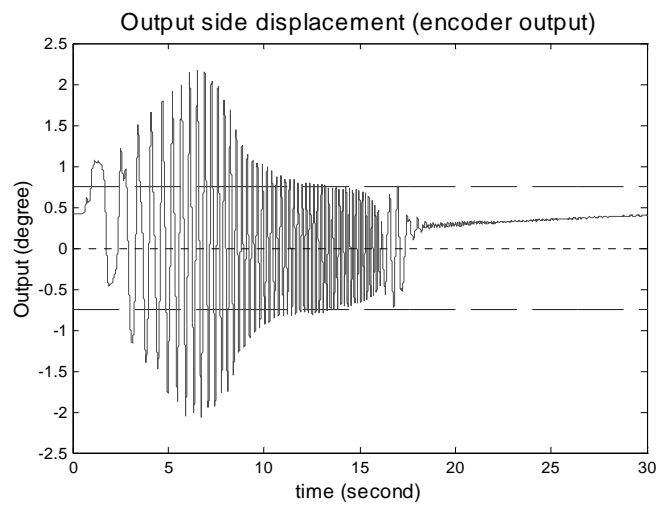


Figure 9. Oscillation measured by encoder #2

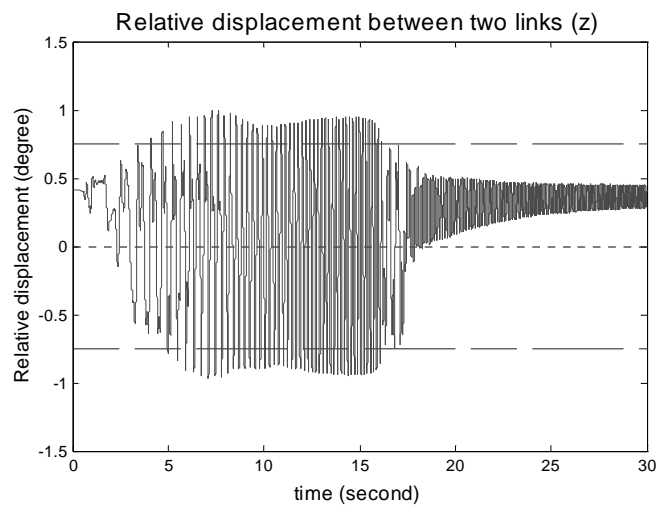


Figure 10. Relative motion between both links (z)

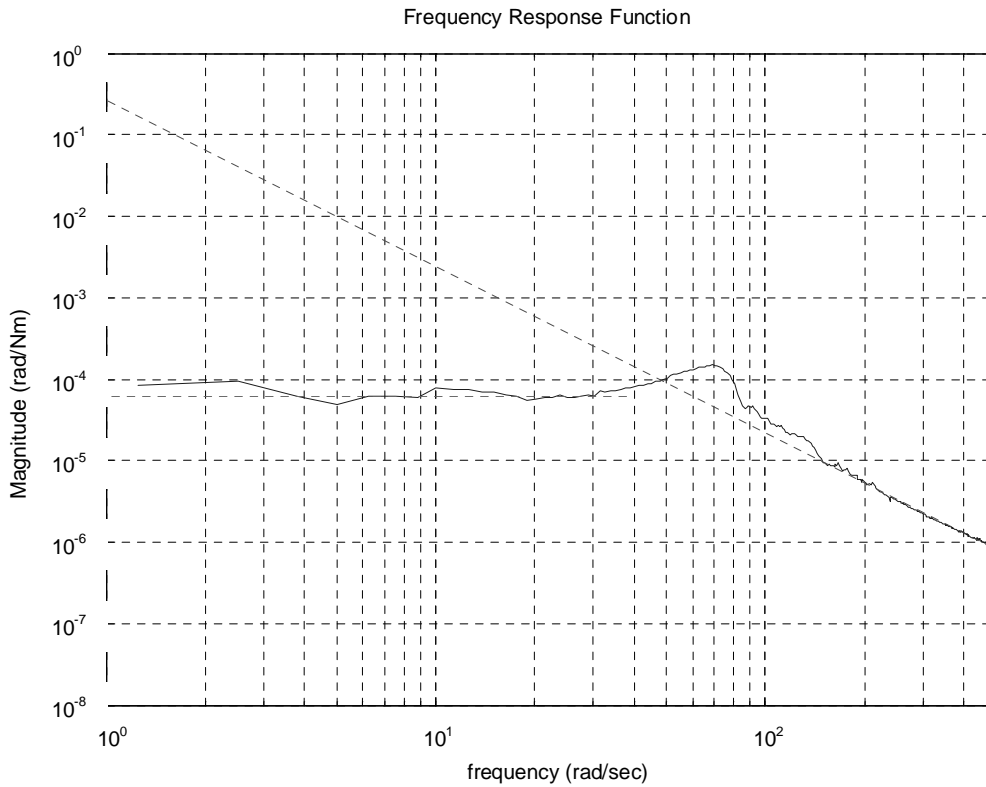


Figure 11. Frequency Response Function of two-link mechanism

In order to check the validity of these identification techniques, the system has been modally identified at the edge of backlash. Figure 11 shows the Frequency Response Function of the system obtained through shock excitation using impact hammer. The link was preloaded using a low stiffness spring to eliminate nonlinearity due to the backlash; hence the link was resting on one of the edges of the backlash. It can be seen from the figure, that the natural frequency of the system is approximately 11 Hz, while from the mass line we can estimate the moment of inertia of the link to be approximately equal to 3.16 kgm^2 . (The estimation of moment of inertia based on its geometric calculation is 2.84 kgm^2 .)

3.1.2 Modification in nonlinear modal parameters calculation

Some obvious modifications of nonlinear modal parameter estimation procedures in equations (2.4) have to be made in order to conform to the base motion case, since we are dealing with displacement input and displacement output in the system.

The displacement input $x(t)$, in complex-analytic form appearing in equation (3.5), can be written as:

$$X(t) = x(t) + j\tilde{x}(t) = B(t) \cdot \exp[j\psi_x(t)]$$

The two derivatives of $X(t)$ are then:

$$\begin{aligned} \dot{X}(t) &= X(t) \left[\frac{\dot{B}(t)}{B(t)} + j\dot{\psi}_x(t) \right] \\ \ddot{X}(t) &= X(t) \left[\frac{\ddot{B}(t)}{B(t)} - \omega_x^2(t) + 2j\frac{\dot{B}(t)}{B(t)}\dot{\psi}_x(t) + j\ddot{\psi}_x(t) \right] \end{aligned}$$

Substituting all of analytic signals and their derivatives in equation (3.5) we can get:

$$\begin{aligned} Z \left\{ \left(\frac{\ddot{A}}{A} - \omega^2 + \omega_0^2 + 2h_0 \frac{\dot{A}}{A} \right) + j \left(2 \frac{\dot{A}}{A} \omega + \dot{\omega} + 2h_0 \omega \right) \right\} = \\ - X \left\{ \left(\frac{\ddot{B}}{B} - \omega_x^2 \right) + j \left(2 \frac{\dot{B}}{B} \omega_x + \dot{\omega}_x \right) \right\} + CY \end{aligned} \quad (3.6)$$

Using the same procedures in equations (2.4) by solving two equations from the real and imaginary parts of equation (3.6), we can obtain the expression for instantaneous modal parameter as functions of first and second derivatives of signal envelopes and instantaneous frequencies of input and output displacement signal.

After identification, the restoring force, which illustrates the nonlinear spring characteristic of the system, and the damping force can be obtained based on the relations:

$$f_s(A) = A \cdot \omega_0^2(A) \tag{3.7}$$

$$f_d(\dot{A}) = 2h_0(A) \cdot \dot{A} \tag{3.8}$$

3.1.3 Identification Result

Envelope and instantaneous frequency calculation of both input (x) and relative output signal (z) can be seen in Figure 12 and Figure 13, respectively. In the left side of both figures, we can see the envelope estimation of displacement input and displacement output. The light-green dashed lines represent the envelope estimation based on Hilbert transform technique without any filtration. The filtered HT curves represent the same technique after low-pass filtration of 0.5% of its half sample rate (100% correspond to half the sample rate), while WT curves represent that of Wavelet Transform technique.

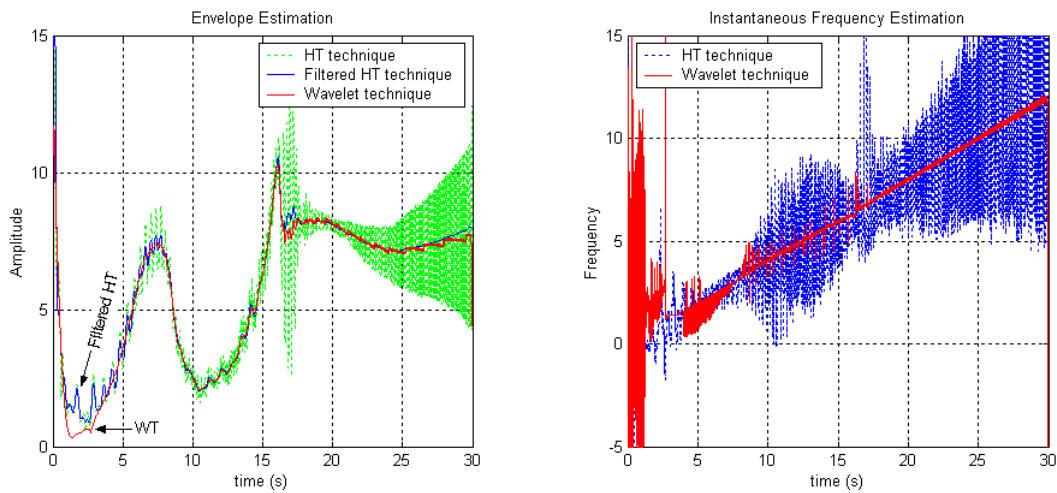


Figure 12. Envelope and instantaneous frequency of input signal

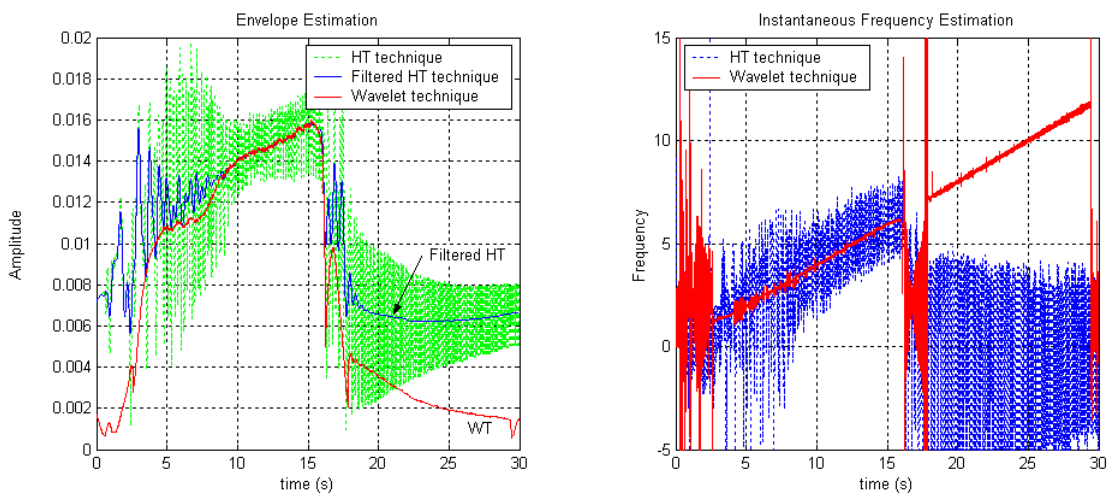


Figure 13. Envelope and instantaneous frequency of output signal

From these two figures, we can see that Wavelet analysis gives an improvement in estimation envelope and instantaneous frequency at several points. The most significant improvement is in the envelope and instantaneous frequency estimation of displacement output approximately after the first 17 seconds. If we refer back to Figure 10, it is clearly seen that the response is shifted after 17 seconds. This might have happened because at the corresponding time, the level of displacement input has fallen below the backlash size in the system. Hilbert Transform technique cannot estimate the envelope and also instantaneous frequency of a signal with certain offset. This is another advantage of Wavelet analysis.

At approximately time 16-17 seconds; we can see a significant estimation error in instantaneous frequency. In this instance, the estimation cannot be made in this region, since the frequency content of vibration response in this instance corresponds to the resonance frequency of the system (refer to Figure 8 and Figure 9).

Restoring Force

The restoring force as function of displacement can be derived utilising equation (2.4a). The plot of this restoring force can be seen in Figure 14. In the left side of Figure 14, we can see the restoring force estimation based on Hilbert transform technique with low-pass filtration of 1% and 0.5% of half of its sample rate, respectively. In the right figure, we see the estimation based on Wavelet analysis. Approximately, the size of backlash obtained from both techniques is close to the real backlash size introduced in the system. From the figures, by applying regression on the reconstructed restoring force, we get the backlash size of 0.0258 rad ($=1.48^\circ$ with standard deviation of error below 1.5%), where the real backlash size is approximately 1.5° from manual measurement.

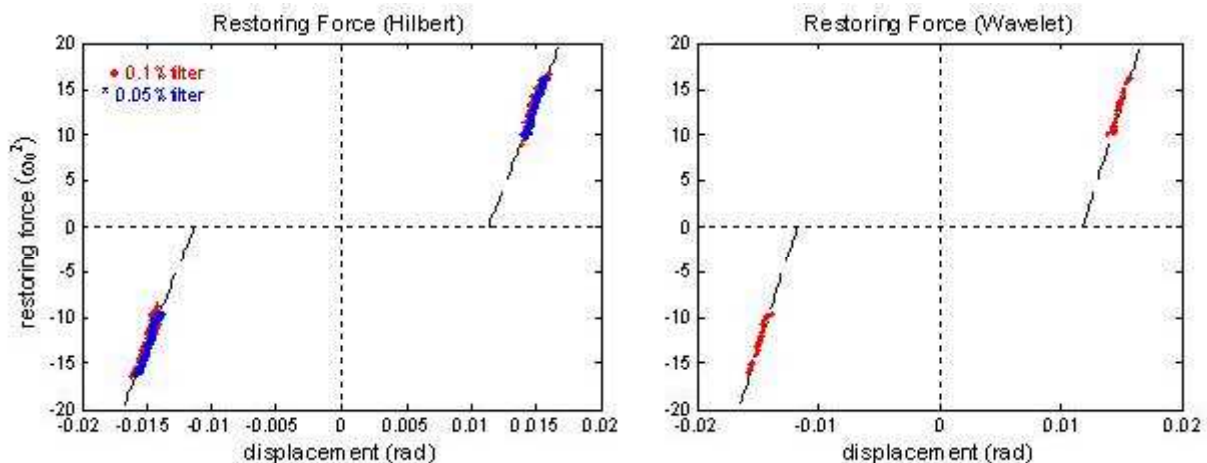


Figure 14. Stiffness force estimation based on Hilbert and Wavelet transform

Referring to equation (2.4a), the slope of the restoring force curve in Figure 14 actually represents the modal stiffness of the system. After multiply the slope by moment of inertia of the second link, we can obtain the estimated stiffness value of the system. Modal stiffness parameter obtained by applying regression to the result approximately is 11000 Nm/rad.

The discontinuity appearing in the figures is due to the response in resonance region as mentioned before. Hence, we cannot obtain the stiffness force estimation in the corresponding region.

3.2 Chaotic behaviour in mechanical system with backlash

So far, identification techniques of structural nonlinearity based on envelope and instantaneous frequencies of vibration response have been discussed in some detail. If the skeleton of a nonlinear structure is measured in the way, which has been discussed in the previous sections then, in case of geometric nonlinearity, the structural nonlinearity can be detected, quantified and identified. However, for some nonlinear systems, under certain excitation regimes, non-periodic response for periodic input (i.e. chaotic response) may arise. Skeleton analysis, which is largely based on the assumption of periodic input

periodic output, becomes then inadequate. In order to analyse the systems in those regimes, the development of more analysis techniques becomes necessary.

Lin [22] shows theoretically that under certain conditions and excitations, a simple mechanical system with backlash might lead to chaotic vibration. Both simulations and experimental results presented in this paper confirm this fact.

Under large amplitude excitation periodic force, it is found that the link system shows non-periodic behaviour as can be observed from Figure 15. For this case, the system was excited by periodic motion with 1.54 Hz fundamental frequency and amplitude of 2.68° .

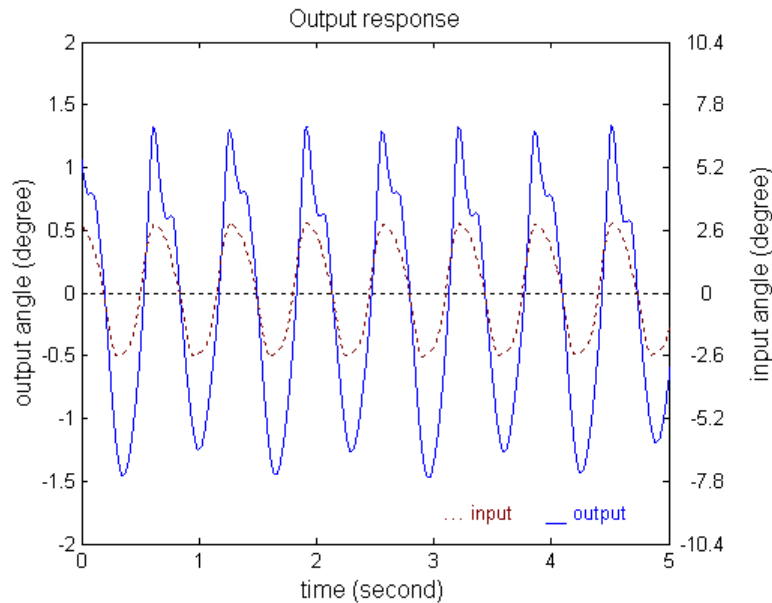


Figure 15. Output response at 1.54 Hz and 2.68° input excitation

To see how chaotic-motion changes when the forcing amplitude increases or the backlash size decreases (as implied by α in dimensional analysis), the corresponding system was excited by different excitation levels ranging from 1.34° to 5.73° , where it was observed that chaotic response persisted.

In this case, again, the displacement measured by encoder#1 was considered as excitation. Figure 16 shows the phase plots of output responses with certain time delay (174), which is determined using the *Average Mutual Information* method [19]. The figures show the evolution of the phase plots when we gradually increase the excitation levels. In particular, bifurcation behaviour is observed with respect to the excitation level. Note that from perspective of dimensional analysis, the change in excitation level is correlated with the backlash size. shows the chaos quantification of Lyapunov exponents, which are obtained after phase space reconstruction as described earlier in section 2.2, for corresponding results in Figure 16, starting from the lowest excitation level to the highest respectively.

<i>Exc. Level</i>	1.34°	2.07°	2.68°	3.41°
<i>Largest Lyap. (bit/time)</i>	0	0	1.423	1.322
<i>Exc. Level</i>	3.65°	3.78°	4.87°	5.73°
<i>Largest Lyap. (bit/time)</i>	1.533	1.802	0	0

Table 2. Chaotic quantification results of series excitation

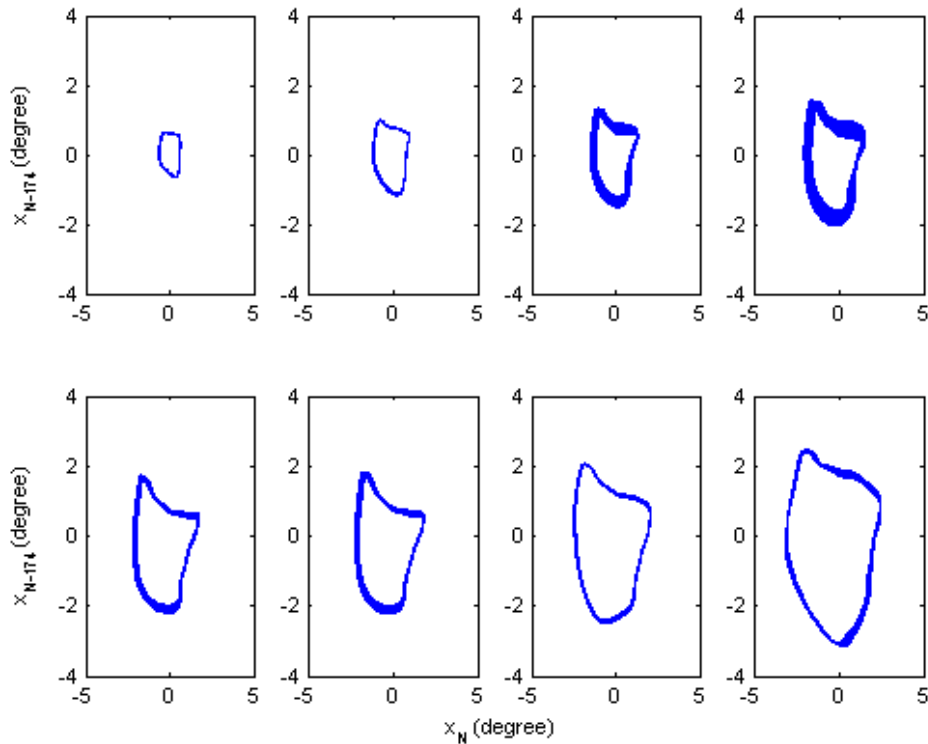


Figure 16. Phase plots of output responses with 174 discrete unit time delay of corresponding mechanical system with excitation frequency of 1.54 Hz and amplitude level respectively from left to right and top to bottom: 1.34°; 2.07°; 2.68°; 3.41°; 3.65°; 3.78°; 4.87°; 5.73°.

Noise Reduction Process

Noise reduction step plays an important role in estimating the largest Lyapunov exponent to quantify chaotic behaviour. The major problem in estimating largest Lyapunov exponent of ‘noisy’ signal concerns to the minimum embedding dimension required to completely unfold the noisy attractor of the signal. Figure 17 shows the result of simple noise reduction method of output response when the system was excited using 3.41° excitation level, compared to the un-cleaned one. One may see that the trajectory appears smoother after noise reduction. Verification and quantification of the noise reduction performance can be done on the basis of the correlation integral [20]. For our case, since the noise level is not significantly high, this verification will not be discussed in this paper.

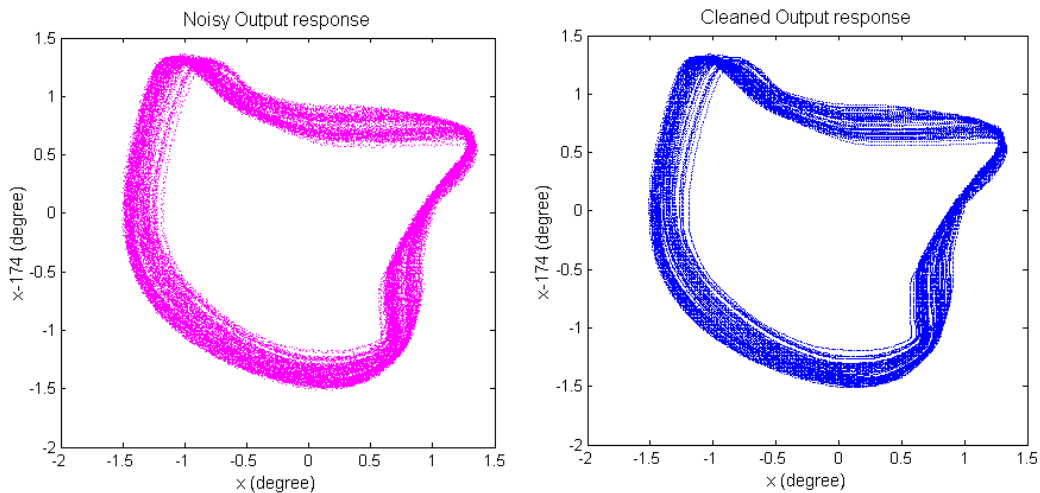


Figure 17. Cleaned signal compared to the noisy one

In Figure 18, we can see the plot of the Cao's number $E1$ versus its embedding dimension d . The solid line represents $E1$ for original noisy signal, while the dash line represents $E1$ for the signal when its noise has been reduced.

Similar to the method of False Nearest Neighborhood, the minimum embedding dimension of any chaotic signal can be concluded by observing the evolution Cao's number $E1$ in its dimension. Cao's number $E1(d)$ will stop changing when the dimension d is greater than the minimum embedding dimension d_0 .

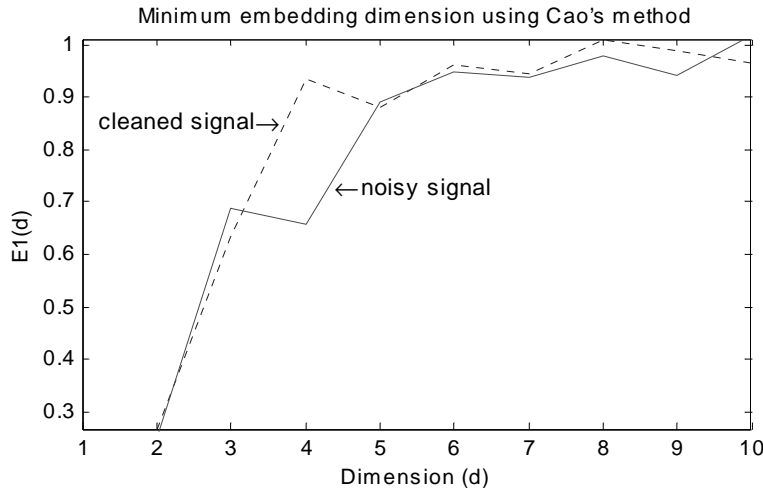


Figure 18. Minimum embedding dimension of noisy and cleaned signals

From Figure 18, we can see that the noisy signal needs a higher dimension to unfold its attractor compared to its cleaned counterpart. The noisy one takes a minimum of 5 embedding dimensions to completely unfold its attractor, while the cleaned one needs only 4.

4 Conclusion

Nonlinear modal parameters estimation technique based on Hilbert and Wavelet transform are shown to be a good approximation of the true modal parameters characteristic. Both the backlash size and the stiffness can be estimated satisfactorily.

An improvement of nonlinear modal parameters estimation by introducing Wavelet analysis has been achieved owing to several advantages offered by Wavelet properties. Wavelet transform is capable of analysing envelope and instantaneous frequency of a shifted signal and the results have less-wiggles compared to those of Hilbert transform. However, there are some drawbacks in the Wavelet based technique. It needs not only a large amount of computation memory for its calculation process, since it deals with time-frequency domain, but also a long processing time.

A major difficulty in utilising the methods introduced in this paper concern the level of displacement input applied to the system. This displacement input should have an adequate level to ensure covering the backlash size. Due to the limitation of energy of excitation, this might become a problem, especially at high frequency. Limited level of displacement input will yield only a partial reconstruction of the restoring force characteristics.

Finally, under certain excitation conditions, there may exist some separate regions for which chaotic vibrations could occur. The transition to and from those regions is marked by bifurcation points. We have shown that, for this case, it would be possible to quantify the Lyapunov exponent, for each amplitude of excitation. Correlating the Lyapunov exponent with $\alpha = A/k_0x_0$ could, in principle, yield the backlash size. Hence, although quite difficult to perform in practice, chaos quantification could be used as a quantitative mechanical signature of a backlash component.

5 References

1. K. Worden, G.R. Tomlinson, *Nonlinearity in Structural Dynamics*, Institute of Physics Publishing, Bristol and Philadelphia, (2001).
2. M. Feldman, S. Braun, *Analysis of Typical Nonlinear Vibration Systems by Using the Hilbert Transform, Proceedings of the XI Int. Modal Analysis Conference., Kissimmee, Florida, (1993)*, pp. 799-805
3. National Instrument website
<http://zone.ni.com/devzone/nidzgloss.nsf/webmain/2579395D1F8016700625687F0061BDF1>
4. G.R. Tomlinson, *Developments in The Use of The Hilbert Transform for Detecting and Quantifying Non-Linearity Associated with Frequency Response Functions*, Mechanical Systems and Signal Processing (1987) 1(2), pp.151-171
5. M. Feldman, *Non-Linear System Vibration Analysis Using Hilbert Transform-I. Free Vibration Analysis Method 'FreeVib'*, Mechanical Systems and Signal Processing (1994) 8(2), pp.119-127
6. M. Feldman, *Non-Linear System Vibration Analysis Using Hilbert Transform-II. Forced Vibration Analysis Method 'ForceVib'*, Mechanical Systems and Signal Processing (1994) 8(3), pp.309-318
7. R.E. Ziemer, W.H. Tranter, *Principle of Communications. Systems, Modulation and Noise.*, Boston: Houghton Mifflin, 1976
8. M. Ruzzene, L. Fasana, L. Garibaldi, B. Piombo, *Natural Frequencies and Dampings Identification Using Wavelet Transform: Application to Real Data*, Mechanical Systems and Signal Processing (1997) 11(2), pp. 207-218
9. M. Misiti, Y. Misiti, G. Oppenheim, J.M. Poggi,, *Wavelet Toolbox for Use with Matlab*, The MathWorks, July 2002 (online only)
10. P.H. Tchamitchian, B. Torr sani, *Ridge and Skeleton Extraction from the Wavelet Transform In Wavelets and Their Application*, in M.B. Ruskai, editor, Jones and Bartlett Publishers, 1992
11. R.A. Carmona, W.L. Hwang, B. Torr sani, *Characterization of Signals by the Ridges of Their Wavelet Transforms*, IEEE Transactions on Signal Processing (1997) 45(10), pp. 2586-2590
12. W.J. Staszewski, *Identification of Nonlinear Systems Using Multy-Scale Ridges and Skeletons of The Wavelet Transform*, Journal of Sound and Vibration (1998) 214(4), pp. 639-658
13. S H. Strogatz, *Nonlinear Dynamics and Chaos*, Addison-Wesley Publishing Company, (1994).
14. A A. Tsonis, *Chaos: From Theory to Applications*, Plerum Press, (1992).
15. R C. Hilborn, *Chaos and Nonlinear Dynamics: An Introduction for Scientist and Engineers*, Oxford University Press, (1994).
16. I. Trendafilova, H. Van Brussel, *Nonlinear Dynamics Tools for The Motion Analysis and Condition Monitoring of Robot Joints*, Mechanical Systems and Signal Processing (2001).
17. L. Cao, A. Mees, K. Judd, G. Froyland, *Determining the Minimum Embedding Dimensions of Input-Output Time Series Data*, International Journal of Bifurcation and Chaos, Vol. 8, No. 7 (1998), pp. 1491-1504.
18. A. Wolf, J.B. Swift, H.L. Swinney, J.A. Vastano, *Determining Lyapunov Exponents From A Time Series*, Physica 16D (1985), pp. 285-317.
19. H. Abarbanel, *Analysis of Observed Chaotic Data*, Berlin: Springer-Verlag, (1996).
20. H. Kantz, T. Schreiber, *Nonlinear Time Series Analysis*, Cambridge University Press, (1997).
21. J. Theiler, S. Eubank, A. Longtin, B. Galdrikian, B., J. Farmer, *Testing for Nonlinearity in Time Series: The Method of Surrogate Data*, Physica 58D, pp. 77-94.
22. R.M. Lin, "*Identification of The Dynamic Characteristics of Nonlinear Structures*", PhD thesis, Mechanical Engineering Department, Imperial College of Science, Technology and Medicine, London (1990).

